PARALLEL-PLATE CAPACITIVE SENSOR FOR SCREENING METHANOL ADULTERATION IN CACHAÇA

Carlos Eduardo Augusto Dias, Jonathan de Matos, Maria Salete Marcon Gomes Vaz
Postgraduate Program in Applied Computing - PPGCA
State University of Ponta Grossa - UEPG

250401401002@uepg.br; jonathan@uepg.br; salete@uepg.br

Abstract: *This paper reports the design, construction, and characterization of a low-cost parallel-plate capacitive sensor intended for screening gross methanol adulteration in cachaça. The transducer, built from copper-clad boards held by a 3D-printed PLA frame, operates without direct fluid–electrode contact: samples are sealed in low-density polyethylene pouches and inserted between the plates. Coupled to an NE555 timer in a stable configuration, the sensor converts changes in the effective permittivity of the medium into oscillation frequency, which is read by a microcontroller through pulse counting. Twenty-eight samples covering 0–30% (v/v) methanol in four commercial cachaças were measured between 15 °C and 26 °C, yielding 2,014 readings. Methanol addition consistently increased the oscillation frequency, consistent with the partial replacement of the high-permittivity aqueous fraction of the beverage by methanol. Univariate linear calibration, however, proved insufficient (best $R^2 = 0.49$): the signal is confounded by a thermal drift of up to −273 counts/°C and by baseline shifts of about 22% caused by dissolved sugars. The results support the hardware as a viable, low-cost data-acquisition platform for adulteration screening and characterize the interferences that any quantification model must compensate, indicating multivariate approaches as the natural next step. The system's selectivity limits and the gap between the tested concentrations and regulatory limits are explicitly discussed.*

Keywords: *cachaça; methanol; capacitive sensor; astable oscillator; dielectric permittivity; low-cost instrumentation.*

1. Introduction

The contamination of alcoholic beverages by methanol constitutes a public health problem due to its toxicity, which can result in damage to the nervous system, blindness, and death (Tian et al. 2022). Episodes of mass poisoning associated with the consumption of adulterated beverages are repeatedly recorded in several countries, including Brazil, highlighting the lack of accessible screening methodologies for controlling this contaminant within the commercialization chain.

Cachaça is a product of economic and cultural relevance for Brazil, deeply tied to the country's history. According to the Ministry of Agriculture and Livestock (MAPA), the product is defined as sugarcane spirit produced in Brazil, with an alcohol content between 38% and 48% by volume at 20 °C, and the addition of sugars up to a limit of 6 g/L is permitted (Brasil 2022; Bezerra et al. 2023). The presence of methanol in cachaça may result from intentional adulteration to maximize profits, but it also occurs naturally as a byproduct of pectin degradation during fermentation; due to its volatility, the compound concentrates in the initial fraction of the distillation process, known as the "head" (Bezerra et al. 2023). These facts justify the implementation of control and inspection tools throughout the entire production and commercial chain of the beverage.

The reference methods for identifying and quantifying methanol—gas chromatography, either isolated or coupled with mass spectrometry—present disadvantages for field inspection: high costs, lack of portability, the requirement for laboratory infrastructure, qualified operators, and prior sample preparation (Tonezzer et al. 2022; Yi et al. 2024). This scenario motivates the development of simple, low-cost screening instruments, such as the one proposed in this paper.

The physical principle explored is dielectric. Cachaça is a hydroalcoholic solution in which water is the major component; at room temperature, water has a dielectric constant of approximately 80, ethanol 24.5, and methanol 32.7 (Bindra and Hazra 2020; Yang et al. 2010). Thus, the substitution of a volume of cachaça—which is dielectrically dominated by water—with methanol decreases the effective permittivity of the mixture and, consequently, the capacitance of a sensor that uses it as a dielectric. Integrated into an astable oscillator, whose period is proportional to capacitance, this effect manifests as an increase in the oscillation frequency, a behavior effectively observed in the experiments reported here.

It is necessary to delimit the scope of the study regarding regulatory limits. Brazilian legislation allows methanol in cachaça only in residual concentrations, on the order of milligrams per 100 mL of anhydrous alcohol (Brasil 2022), which corresponds to volume fractions much lower than 0.1% of the beverage. The concentrations evaluated in this study, from 2% to 30% (v/v), are therefore orders of magnitude above the legal limit and correspond to scenarios of gross adulteration, such as the fraudulent substitution of part of the distillate with methanol. The system described herein should be understood as a proof of concept for screening instrumentation for this type of fraud, rather than a method for quantifying methanol at regulatory or toxicological levels.

The objective of this article is to describe the design, construction, and characterization of a low-cost parallel-plate capacitive sensor, operated at room temperature and without direct contact between the fluid and the electrodes. Additionally, it seeks to identify and quantify the factors—such as thermal drift and matrix composition—that limit the univariate calibration of the instrument and must be compensated for by multivariate models in future works.

2 Literature Review

2.1 Methanol Detection

Related works involve emerging technologies attempting to bypass the operational limitations of traditional methods. Among conventional approaches, spectroscopic techniques demand high-cost optical equipment and present difficulties regarding miniaturization (Yi et al. 2024). Solutions based on electronic noses with semipermeable polymeric membranes (Kim et al. 2024) or on graphene-based volatile organic compound (VOC) sensors (Capman et al. 2024) show promise, but struggle with signal overlap stemming from the similar electric dipole moments of ethanol and methanol, which compromises selectivity.

Within the scope of metal oxide nano sensors, devices based on tin dioxide nanowires (Tonezzer et al. 2022) and titanium dioxide nanotubes (Bindra and Hazra 2020) stand out. The implementation of these technologies, however, depends on highly complex and expensive microfabrication processes, such as electrochemical anodization and the deposition of gold contacts via vacuum thermal evaporation (Bindra and Hazra 2020).

The literature also proposes sensors based on CMOS capacitive arrays, with measurements of the sample evaporation time (Osouli Tabrizi et al. 2024), and interdigital structures (IDE) manufactured on printed circuit boards (Costa et al. 2022). Although offering a simplified manufacturing route, systems like IDEs require the integration of micro test chambers and dedicated heating circuits (Costa et al. 2022). This requirement exposes a recurring limitation: thermal dependency. Metal oxide or thermal gradient sensors require elevated operating temperatures, in ranges from 30 °C to 300 °C (Tonezzer et al. 2022) or from 50 °C to 225 °C (Chowdhury and Bhowmik 2022), to stabilize the signal and

distinguish the analytes, which raises energy consumption and restricts their use in portable field devices (Tonezzer et al. 2022).

As an alternative to solid-state components, there is the biosensor route, which operates by immobilizing the alcohol oxidase (AOX) enzyme in sensing matrices (Razmshoar et al. 2023). Despite their high biological selectivity to methanol, the use of organic elements faces physicochemical instability: the activity and structure of the enzyme are compromised by variations in temperature, humidity, and pH, restricting the sensor's robustness and lifespan outside of controlled environments (Razmshoar et al. 2023).

2.2 Capacitive Sensing and Dielectric Properties

The capacitance (C) of a parallel-plate capacitor is directly proportional to the area of the conductive surfaces (A) and inversely proportional to the distance between them (d), with this quotient multiplied by the permittivity of the dielectric material (ε) present between the plates (Robbins and Miller 2013):

$$C = \frac{\epsilon A}{d} \quad (1)$$

In the experimental setup, the sample fluid acts as the dielectric, filling the cavity between the armatures, replacing air. The feasibility of sensing stems from the divergence of the dielectric constants of the pure components at room temperature: water (≈ 80), methanol (≈ 32.7), and ethanol (≈ 24.5) (Bindra and Hazra 2020; Yang et al. 2010). Altering the proportion among these components modifies the effective permittivity and relaxation time of the mixture, altering the capacitance measured by the circuit and enabling the physical discrimination of the compositions exclusively via the electric field (Yang et al. 2010). It should be noted that this is a bulk measurement of the mixture, with no intrinsic chemical selectivity mechanism, an implication discussed in Section 4.4.

2.3 Electronic Instrumentation and Capacitance–Frequency Conversion

Measuring capacitances on the order of picofarads demands high resolution and noise mitigation, a challenge in purely analog interfaces due to parasitic capacitances and interferences (Gasulla et al. 2005). Interfaces whose output signals are frequency-modulated emerge as a solution, as they can be connected directly to microcontrollers (Gasulla et al. 2005). Their implementation is simplified through relaxation oscillators, such as the NE555 timer integrated circuit in astable mode (Vuković Rukavina 2014).

In this topology, the capacitive sensor is inserted into the oscillator's timing stage: changes in the dielectric's permittivity modify the charge and discharge times, converting capacitance variations directly into the frequency domain (Vuković Rukavina 2014). The modulated signal exhibits good immunity to transmission noise and allows processing through pulse counting in microcontrollers, such as those from the Arduino platform (Gubsky 2023), enabling low-cost analytical instrumentation with sufficient robustness for field measurements (Gasulla et al. 2005; Gubsky 2023).

3. Material and Methods

3.1. Parallel-Plate Capacitive Sensor

Exploring the dielectric properties described in Section 2.2, a device was constructed whose capacitance varies according to the fluid introduced inside it, termed the Parallel-Plate Capacitive Sensor. As a base structure, 5 cm × 5 cm copper-clad printed circuit boards

(PCBs) were used. Two practical challenges needed addressing: ensuring parallel alignment between the plates and establishing an efficient method for fluid sample insertion.

Preliminary tests, though partially unsuccessful, are recorded here for their design value. An assembly with 0.2 mm spacers manufactured via Fused Deposition Modeling (FDM, commonly known as "3D printing") using polylactic acid (PLA) filament was tested, aligned between the copper plates and secured by plastic clamps, with the direct injection of liquid into the cavity. This configuration served as a proof of concept: capacitance measurements showed that pure and adulterated cachaça samples produced low, yet distinguishable, capacitances.

The mechanism, however, proved impractical for two reasons: the pressure from the clamps was insufficient to seal the assembly, causing leaks; and the direct contact of the liquid with the conductors required rigorous disassembly and cleaning after each reading to avoid cross-contamination—an operational challenge regarding degradation and analytical drift well-documented in the literature for direct-contact sensors (Vuković Rukavina 2014; Bindra and Hazra 2020; Kim et al. 2024).

These reasons prompted changes to the mechanical structure and the sample insertion method. A structure was developed using FDM in PLA, equipped with guide rails into which the plates are fitted, kept parallel with a fixed 2 mm spacing. The literature supports the use of this manufacturing technique and polymer for enabling physical systems without complex machinery, resulting in a mechanically stable and low-cost support (Gothard et al. 2023). The design is presented in Figure 1, with one of the plates detached to show its dimensions; the final configuration, with the plate positioned and the spacing dimension, is shown in Figure 2. Alongside the parallel conductive area, a linear copper strip was provided for attaching a conductive wire, allowing the sensor to be connected to electronic circuits.

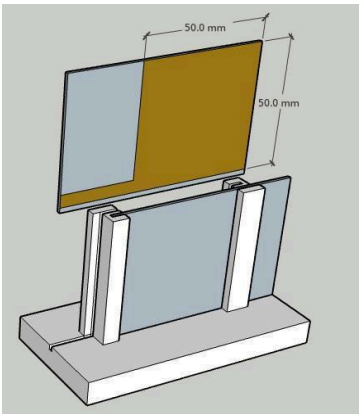

Figure 1: Structural design of the sensor
Source: The Authors

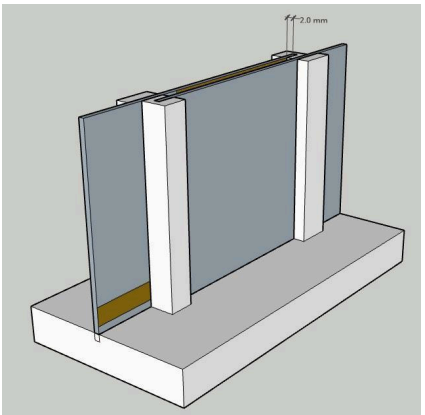

Figure 2: Plate spacing of the Sensor
Source: The Authors

To insert the samples without direct contact with the conductors, the use of plastic containments was evaluated. Low-density polyethylene (LDPE, zip-lock type) pouches of 5 cm × 8 cm were adopted, into which 7 mL of solution was packed. The sealed pouches were positioned in the measurement space between the plates, and it was observed that, even with the LDPE barrier, different compositions continued to produce distinct and measurable variations in capacitance. This behavior is consistent with the penetration of electric field lines through solid and polymeric dielectric barriers, which enables non-contact capacitive sensing (Sattari and Hayati 2024; Vuković Rukavina 2014). Figure 3 shows a filled pouch; Figure 4 demonstrates its insertion into the sensor.

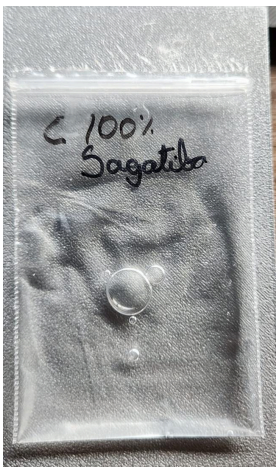

Figure 3: Example of a sample in an LDPE pouch
Source: The Authors

Figure 4: Demonstration of the sample being inserted into the sensor
Source: The Authors

3.2 Data Acquisition Circuit

Once the sensor's response was verified on the bench, efforts were focused on converting the capacitance variations into signals processable by microcontrollers. The acquisition system is based on the NE555P timer integrated circuit in astable oscillator mode, chosen for its low cost, its suitability for portable architectures, and its ability to convert capacitance changes directly into the frequency domain (Vuković Rukavina 2014). The technique mitigates the effect of parasitic capacitances and favors immunity to coupling noise (Gasulla et al. 2005); additionally, the pulsed signal eliminates the need for high-precision analog-to-digital converters, allowing direct integration with microcontroller internal counters (Gasulla et al. 2005; Vuković Rukavina 2014).

The circuit was powered by a 5 V direct current (DC) supply provided by the Arduino's USB interface. A 10 nF auxiliary bypass capacitor was connected to the control voltage pin (Pin 5) of the NE555P to ensure stability and mitigate reference noise. The conversion was validated by analyzing the timer's output signal on a digital oscilloscope model Fnirsi Dso510 Plus.

The conversion was validated by analyzing the timer's output signal on an oscilloscope. Figures 5 and 6 display the waveforms at the NE555P output with the sensor coupled to the timing stage, containing, respectively, a cachaça sample with no added methanol (0%) and a sample with 30% (v/v) methanol. The measured frequencies—285.71 kHz for the pure sample and 291.46 kHz for the adulterated sample—highlight the distinction of the signals and the direction of the effect: the addition of methanol decreases the effective permittivity of the medium (Section 1), which reduces capacitance and raises the oscillation frequency.

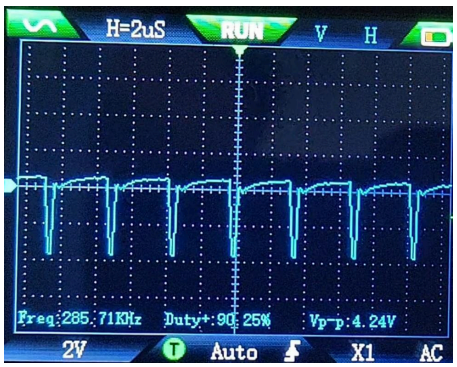

Figure 5: NE555P IC output waveform for pure cachaça sample (100%).
Source: The Authors

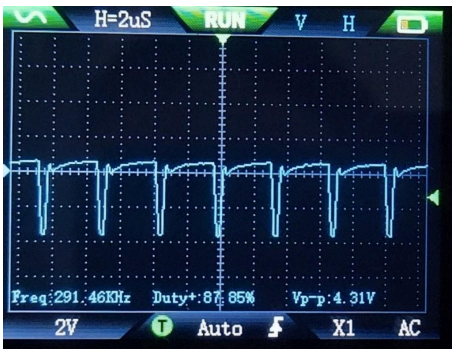

Figure 6: NE555P IC output waveform for contaminated sample (70%)
Source: The Authors

Aiming to enrich data collection, the architecture included dynamic switching of resistances in the charge branch (R_1) of the NE555P, while maintaining the discharge branch (R_2) constant at 1 kΩ. A set of three physical resistors (10 kΩ; 4.7 kΩ; 1 kΩ) was used, which, through parallel associations, provided two additional equivalent resistances (3.19 kΩ and 824 Ω), totaling five distinct RC time constants. Collection under different stimulus frequencies is justified because polar components, such as methanol and ethanol, present distinct orientational polarization dynamics (Chowdhury e Bhowmik 2022); switching allows mapping the sensor's response against resistive losses, producing a richer dielectric signature for future algorithmic classification (Chowdhury e Bhowmik 2022). The internal operation of the NE555P is illustrated in Figure 7.

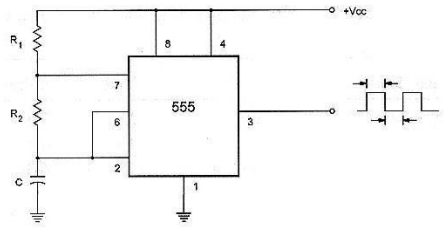

Figure 7: Operating diagram of the NE555P IC.
Source: The Authors

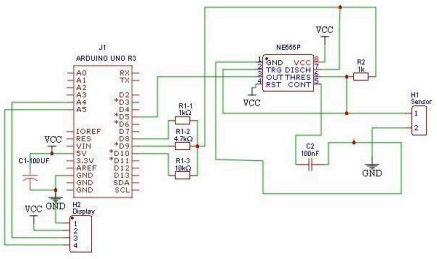

***Figure* 8: Schematic of the electronic circuit for data collection**
Source: The Authors

For acquiring and processing the frequencies, the NE555P output was connected to a microcontroller-based prototyping board (Arduino Uno R3), whose use for instrumentation and signal reading is validated in the literature (Gubsky 2023). A C-language algorithm counted the digital pulses produced by the oscillator in fixed time windows; each dataset record corresponds to the number of pulses counted in one window (counts per window, CPW). The complete system topology is detailed in Figure 8.

3.3. Samples and Experimental Design

Four commercial brands of cachaça with varied physicochemical characteristics were selected, identified here as Brands A, B, C, and D, to evaluate the system's behavior regarding different base matrices. The specifications of each base sample—commercial

classification, declared presence of sugars, and a comparison between the labeled alcohol content and the content measured on the bench—are shown in Table 1.

The selection of distinct physicochemical matrices prioritized variability in sugar concentration. Although the exact amount is not declared on labels, the product's legal framework allows inferring the profiles (Brasil 2022): beverages marketed as "cachaça" that report the presence of sugar comply with the regulatory maximum of 6 g/L; products labeled as "sweetened cachaça" contain levels above this limit, in exact concentrations unknown to the consumer (Brasil 2022). The presence of sugars reflects market practices; adding sweeteners is used in spirits to disguise the taste of lower-quality beverages (Yi et al. 2024), and it can also occur secondarily, such as through the dissolution of fruit compounds stored in the bottle (Bezerra et al. 2023). This deliberate variation in the composition of the base samples allows evaluating the system's behavior toward fluids with distinct dielectric characteristics.

The divergence between the labeled and measured alcohol content (Table 1) is explained by the physical measurement method. Bench readings were taken with a Gay-Lussac alcoholometer, whose principle relies on the fluid's overall density. In water and alcohol mixtures, ethanol reduces the solution's density (Plugatar et al. 2023); however, sugars and dissolved solids raise the density, counteracting the effect of the alcohol and generating greater buoyancy on the hydrometer (Plugatar et al. 2023). Direct densimetry, therefore, records the "apparent alcoholic strength," which is systematically lower than the actual content in sweetened beverages (Guimarães 2013); in these cases, determining the true strength requires prior distillation (Bezerra et al. 2023). The measured values are reported here merely as a qualitative characterization of the matrix, and not as a determination of the true alcohol content.

Twenty-eight samples were prepared, corresponding to seven levels of methanol addition for each of the four brands. Each LDPE pouch was filled with a fixed total volume of 7 mL, with the mixtures composed in volumetric methanol proportions of 0% (pure cachaça), 2%, 5%, 10%, 15%, 25%, and 30% (v/v), with the remainder of the volume consisting of the base cachaça.

Temperature variation was also incorporated into the experimental design. The literature establishes that the permittivity of polar liquids decreases with heating, as thermal agitation hinders the alignment of molecules with the alternating electric field (Mayet et al. 2023; Yang et al. 2010). Measurements were conducted under thermal conditions between 15 °C and 26 °C, with direct measurement taken by a thermometer immersed in the fluid—rather than relying on ambient temperature—ensuring correspondence with the liquid under analysis.

Consolidation of the tests resulted in 2,014 (two thousand and fourteen) records, covering the combinations of brand, methanol addition level, resistor configuration, and thermal condition. It is emphasized that these records constitute repeated readings of the 28 physical sample units, and not independent observations, which is considered in the statistical interpretation (Section 4). To enable continuous and automated collection, the information transmitted by the microcontroller was received by a computer running a Python script, tasked with capturing the counts, associating them with the sample labels and temperature, and structuring them into a CSV file, generating the definitive research dataset.

4. Results and Discussion

4.1 Direction of Effect and Frequency–Period Relationship

In astable oscillators, capacitance has an inversely proportional relationship to frequency ($f \propto 1/C$) and a directly proportional relationship to period ($T \propto C$, where $T = 1/f$). Consistent with the mechanism proposed in Section 1—substitution of the high-permittivity aqueous fraction with methanol—the addition of the contaminant raised the oscillation frequency in all evaluated conditions, as illustrated in Figures 5 and 6 (285.71 kHz for 0% and 291.46 kHz for 30% v/v of methanol).

The signal response was evaluated using univariate linear regressions relating the methanol concentration to the circuit's output, restricting the thermal range to 20–23 °C to reduce the influence of temperature (Brand C). Table 2 presents the coefficients of determination (R^2) for the five resistor configurations, comparing the raw frequency data with those converted to period.

Table 2 – Coefficients of determination (R^2) of univariate regressions concentration × signal, for frequency and period (Brand C; 20 °C to 23 °C).

Resistor (R_1)	R^2 (frequency)	R^2 (period)
10 kΩ	0,4832	0,4873
4,7 kΩ	0,3958	0,3953
3,19 kΩ	0,4461	0,4456
1 kΩ	0,3229	0,3221
824 Ω	0,3212	0,3204

Source: The Authors

The results indicate a measurable, yet weak response, insufficient for univariate calibration: even in the best configuration (10 kΩ), the linear model explains less than half of the signal variance (R^2) = 0.49), despite a restricted thermal range. The differences between the R^2) of frequency and period are marginal (e.g., 0.4832 against 0.4873) and do not, in isolation, justify preferring one of the representations. It is also noted that the R^2) values were calculated over repeated readings of the same sample units, which tends to overestimate the apparent precision of the fits; future analyses must aggregate the readings by sample or employ repeated measures models.

For the 10 kΩ configuration (Brand C), the overall univariate sensitivity was 84.09 counts per percentage point of methanol (95% CI: 78.74 to 89.43 counts/%). The standard deviation of the blank (pure cachaça) was 254.48 counts. Using the 3.3σ criterion, the estimated Limit of Detection (LOD) for this univariate approach was 9.98% (v/v) methanol. This high LOD mathematically illustrates why simple linear calibration is insufficient for regulatory compliance, as it is heavily inflated by the uncompensated thermal variance. Figure 9 presents the scatter plot of the signal against methanol concentration, evidencing the linear trend alongside the significant dispersion caused by temperature.

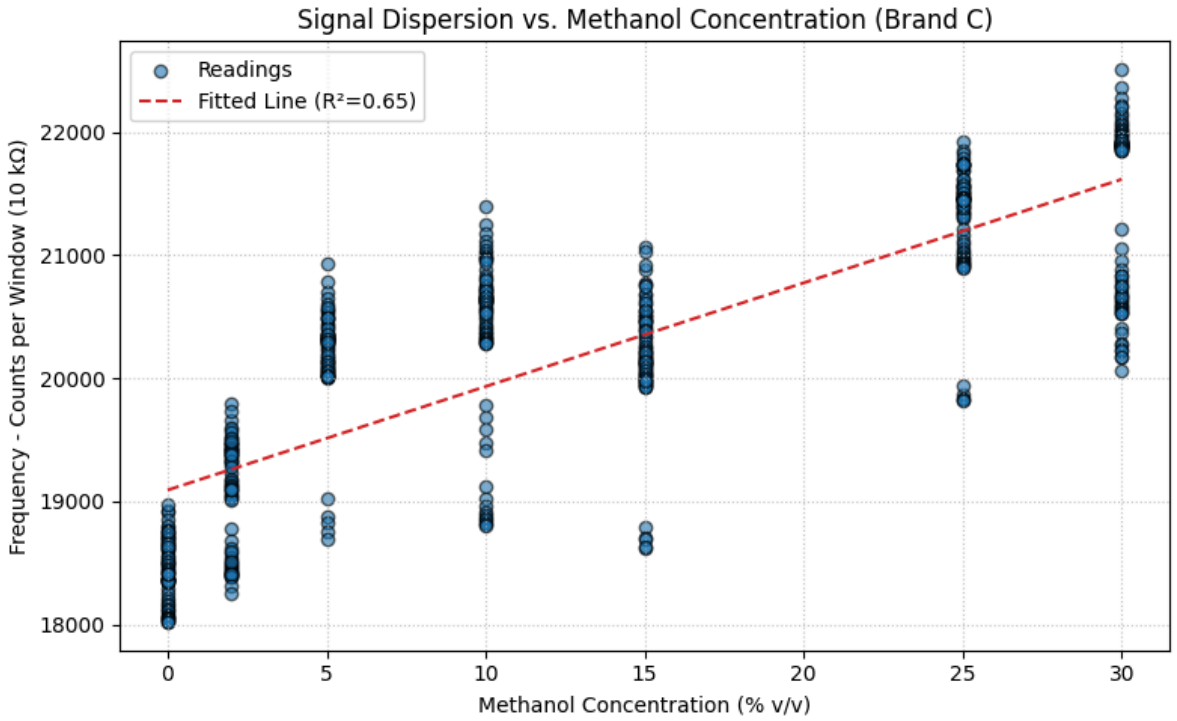

Figure 9: Scatter Plot of Signal Against Methanol Concentration
Source: the authors.

4.2 Influence of the Cachaça's Physicochemical Matrix

The impact of the beverages' base composition on the transducer reading was then evaluated by comparing samples without methanol addition (0%), in the 20 °C to 22 °C range with a 10 kΩ resistor, aiming to characterize the baseline count of each matrix. Table 3 presents the average pulse counts per window.

Table 3 – Average counts per window by brand (samples without methanol; 10 kΩ resistor; 20–22 °C).

Brand	Mean	Std. Dev.
A (standard cachaça)	20,547.27	424.85
B (sweetened cachaça)	15,762.18	267.59
C (Standard Cachaça)	18,457.06	254.48
D (Artisanal Cachaça)	16,389.63	207.73

Source: The Authors

An analysis of variance (ANOVA) confirmed that the baseline shift between the four commercial brands is statistically significant ($F(3, 280) = 3716.98$, $p < 0.001$).

The sample with declared sugar addition (Brand B) presented a level 4,420.90 counts lower than that of the standard cachaça (Brand A), a reduction on the order of 22%. The concentration of soluble solids alters the effective permittivity of the base fluid (Plugatar et al. 2023; Bezerra et al. 2023), shifting the signal baseline by a magnitude comparable to, or

greater than, the variation induced by the methanol itself. This characterizes the matrix composition as a first-order interferent for any universal calibration.

4.3 Thermal Drift

Temperature directly affects the system's reading: its elevation alters the polarization dynamics of the liquid's molecular dipoles and, consequently, the matrix's permittivity (Mayet et al. 2023; Yang et al. 2010). To quantify the effect, Brand C was isolated at the 0% and 30% (v/v) methanol levels, evaluating the count as a function of temperature (Figure 10).

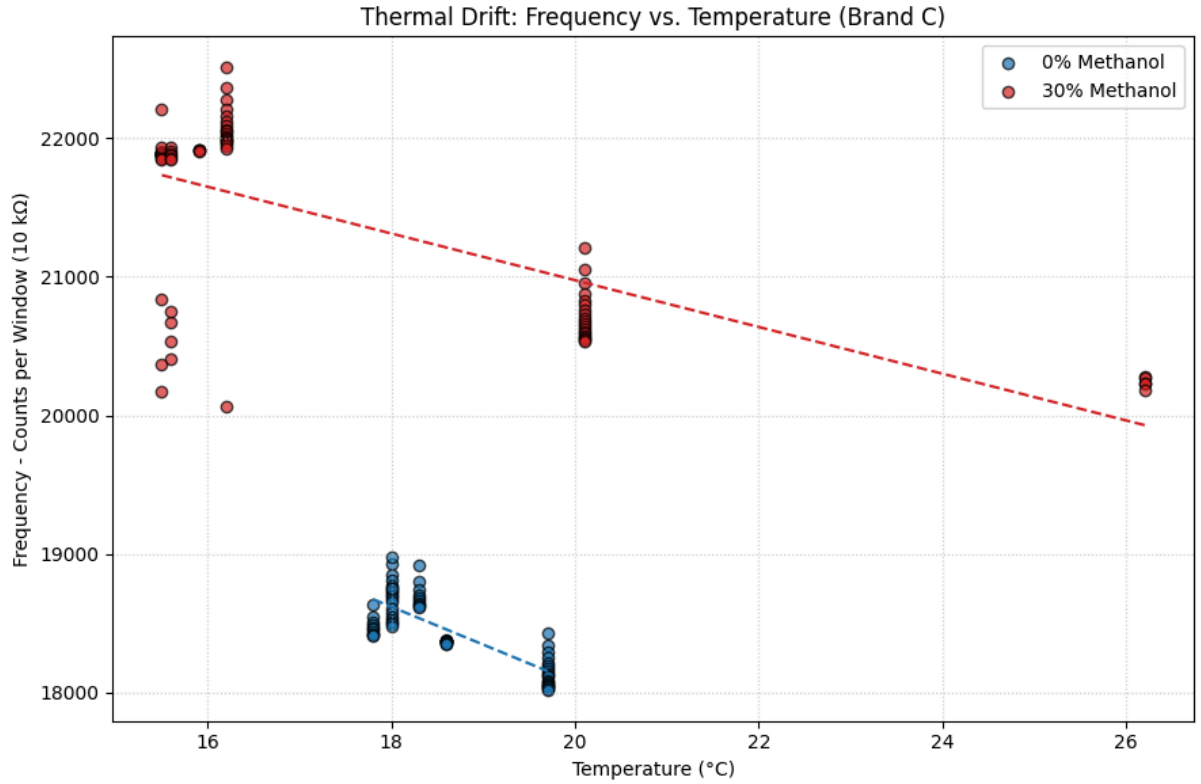

Figure 10: Thermal drift of the signal for cachaça samples without methanol (0%) and with 30% (v/v) methanol (Brand C; 10 kΩ resistor).
Source: the authors.

Linear regression of the sample without methanol revealed a drift of 273.12 counts per degree Celsius ($R^2 = 0.6458$); the sample with 30% methanol recorded a drift of 168.77 counts per degree Celsius ($R^2 = 0.4792$). Consequently, temperature variation causes an overlap in the count ranges among samples with distinct adulteration levels: a heated pure sample may register counts equivalent to those of a cold adulterated sample, rendering any univariate calibration curve that ignores temperature unviable.

It should be noted that the sign of the observed drift is opposite to that expected by the simplified dielectric model: if heating reduces permittivity (Mayet et al. 2023; Yang et al. 2010), capacitance should decrease, causing the frequency—and therefore the count—to increase with temperature, rather than decrease, as observed. This behavior suggests the presence of competing mechanisms not captured by the purely capacitive model, among them: the increase in ionic conductivity and dielectric losses of the hydroalcoholic medium with temperature, which imposes an additional load on the timing stage; dimensional variations of the PLA structure and the LDPE pouch; and the thermal dependence of the circuit components themselves (NE555 and resistors). Investigating and separating these mechanisms is a necessary step for future work; for the purposes of this study, the result establishes temperature as a mandatory covariate for any quantification model.

4.4 Study Limitations

Four limitations bound the scope of the conclusions. First, the evaluated concentrations (2% to 30% v/v) are orders of magnitude above the regulatory limits for methanol in cachaça; the results support screening for gross adulteration, but assert nothing regarding the detection of methanol at legal compliance levels.

Second, by measuring a global dielectric property of the mixture, the sensor lacks intrinsic chemical selectivity. Changes in composition unrelated to methanol, dilution with water, variation of ethanol content within the legal range of 38% to 48%, or sugar addition, also shift the signal, as demonstrated in Section 4.2. Without control tests in which equivalent volumes of water or ethanol replace the cachaça, it is not possible to attribute the observed variation specifically to methanol; such tests are indispensable moving forward.

Third, the 2,014 (two thousand and fourteen) records stem from only 28 physical sample units, meaning the presented statistics reflect repeated readings, not independent replicates. The creation of true replicates (multiple pouches per condition) is necessary to estimate the method's actual variability, and is a prerequisite for future machine learning models to be trained and validated without data leakage between partitions. Fourth, the variability introduced by the LDPE pouch (thickness, bubbles, positioning) was not quantified and may account for a relevant portion of the observed dispersion.

5. Conclusion

This study documented the development and characterization of a low-cost parallel-plate capacitive sensor for screening gross methanol adulteration in cachaça. Additive manufacturing in PLA and LDPE pouches made it possible to measure variations in the effective permittivity of the fluids without direct contact with the electrodes, and integration with the NE555P oscillator fulfilled the instrumentation objective, converting capacitance changes into frequency signals processable by a microcontroller.

The tests confirmed the hardware's capability to register modifications in the dielectric medium caused by the addition of the contaminant, with an effect direction consistent with the replacement of the beverage's aqueous fraction by methanol. Univariate calibration, however, proved insufficient: the best linear fits achieved an R^2 of only 0.49, and two first-order interferents were quantified: the baseline shift caused by dissolved sugars (a reduction on the order of 22% in counts between a standard and a sweetened cachaça) and thermal drift (up to −273 counts/°C), whose direction—opposite to that predicted by the purely capacitive model—indicates the added impact of conductive losses and circuit effects.

The quantification problem is, therefore, multidimensional: frequency, temperature, and base matrix must be addressed jointly. The instrumentation literature supports the use of machine learning techniques in capacitive sensors to address nonlinearities (Sattari and Hayati 2024; Höfler 2024), compensate for thermal drift (Han et al. 2020; Al-Fayoumi et al. 2023), and isolate the variable of interest amidst noise that renders simple linear methods unfeasible (Zimmerman et al. 2018; Capman et al. 2024; Kumar and Sahu 2021). Future works will encompass: (i) control tests with water and ethanol to characterize selectivity; (ii) independent physical replicates and the quantification of pouch variability; (iii) validation of concentrations by gas chromatography; and (iv) the training and validation of multivariate

models—ranging from multiple regressions and PLS to machine learning algorithms—on the generated dataset, with partitioning by sample unit.

Declaration

Conflict of interest: the authors declare no conflict of interest. The commercial brands used were anonymized; the addition of methanol to the samples was carried out exclusively in the laboratory for experimental purposes and does not reflect the composition of the commercial products.

References

Al-Fayoumi, M. A.; Al-Mimi, H. M.; Veisi, A.; Al-Aqrabi, H.; Daoud, M. S.; Eftekhari-Zadeh, E. Utilizing artificial neural networks and combined capacitance-based sensors to predict void fraction in two-phase annular fluids regardless of liquid phase type. *IEEE Access*, 2023. https://doi.org/10.1109/ACCESS.2023.3340127.

Bezerra, F. A. et al. Avaliação dos parâmetros físico-químicos de aguardente de abacaxi produzida e de cachaças comercializadas no Tocantins. *Journal of Biotechnology and Biodiversity*, v. 11, n. 1, p. 39–44, 2023.

Bindra, P.; Hazra, A. Dielectric sensor system using TiO2 nanotubes for real-time detection of methanol contamination in alcoholic beverages. *IEEE Transactions on Instrumentation and Measurement*, v. 69, n. 9, p. 6621–6629, 2020. https://ieeexplore.ieee.org/document/8995480.

Brasil. Ministério da Agricultura, Pecuária e Abastecimento. Portaria MAPA nº 539, de 26 de dezembro de 2022. Estabelece os padrões de identidade e qualidade da aguardente de cana e da cachaça. *Diário Oficial da União*, Brasília, DF, 27 dez. 2022. Seção 1, p. 13.

Capman, N. S. S. et al. Using machine learning to overcome interfering oxygen effects in a graphene volatile organic compound sensor. *ACS Applied Materials & Interfaces*, v. 16, p. 7554–7564, 2024. https://doi.org/10.1021/acsami.3c16641.

Chowdhury, N. K.; Bhowmik, B. Sensing performance of Ti/TiO2 nanosheets/Au capacitive device: implication of resonant frequency. *Solid-State Electronics*, v. 194, 108383, 2022. https://doi.org/10.1016/j.sse.2022.108383.

Costa, J. P. C. et al. Graphite-based multianalyte VOC gas detection on multichannel PCB IDE sensor. *IEEE Sensors Journal*, v. 22, n. 22, p. 22089–22097, 2022. https://ieeexplore.ieee.org/document/9893116.

Gasulla, M.; Li, X.; Meijer, G. C. M. The noise performance of a high-speed capacitive-sensor interface based on a relaxation oscillator and a fast counter. *IEEE Transactions on Instrumentation and Measurement*, v. 54, n. 5, p. 1934–1941, 2005. https://doi.org/10.1109/TIM.2005.853684.

Gothard, A. T.; Hott, J. W.; Anton, S. R. Dynamic characterization of a low-cost fully and continuously 3D printed capacitive pressure-sensing system for plantar pressure measurements. *Sensors*, v. 23, n. 19, 8209, 2023. https://doi.org/10.3390/s23198209.

Gubsky, S. Development of low-cost Arduino-based equipment for analytical and educational applications. *Engineering Proceedings*, v. 48, n. 1, 8, 2023. https://doi.org/10.3390/CSAC2023-14883.

Guimarães, R. A. *Produção de aguardente utilizando o sorgo sacarino (Sorghum bicolor (L.) Moench)*. Tese (Doutorado em Ciências Biológicas) — Universidade Federal de Ouro Preto, Ouro Preto, 2013.

Han, Z.; Hong, L.; Meng, J.; Li, Y.; Gao, Q. Temperature drift modeling and compensation of capacitive accelerometer based on AGA-BP neural network. *Measurement*, v. 164, 108019, 2020. https://doi.org/10.1016/j.measurement.2020.108019.

Höfler, L. Good results from sensor data: performance of machine learning algorithms for regression problems in chemical sensors. *Sensors and Actuators B: Chemical*, v. 421, 136528, 2024. https://doi.org/10.1016/j.snb.2024.136528.

Kim, J. Y. et al. Practical organic electronic noses using semi-permeable polymer membranes. *Applied Materials Today*, v. 37, 102137, 2024. https://doi.org/10.1016/j.apmt.2024.102137.

Kumar, V.; Sahu, M. Evaluation of nine machine learning regression algorithms for calibration of low-cost PM2.5 sensor. *Journal of Aerosol Science*, v. 157, 105809, 2021. https://doi.org/10.1016/j.jaerosci.2021.105809.

Mayet, A. M. et al. An artificial neural network and a combined capacitive sensor for measuring the void fraction independent of temperature and pressure changes for a two-phase homogeneous fluid. *Flow Measurement and Instrumentation*, v. 93, 102406, 2023. https://doi.org/10.1016/j.flowmeasinst.2023.102406.

Osouli Tabrizi, H.; Forouhi, S.; Azadmousavi, T.; Ghafar-Zadeh, E. A multidisciplinary approach toward CMOS capacitive sensor array for droplet analysis. *Micromachines*, v. 15, n. 2, 232, 2024. https://doi.org/10.3390/mi15020232.

Plugatar, Y.; Johnson, J. B.; Timofeev, R. et al. Prediction of ethanol content and total extract using densimetry and refractometry. *Beverages*, v. 9, n. 2, 31, 2023. https://doi.org/10.3390/beverages9020031.

Razmshoar, P. et al. A conductometric enzymatic methanol sensor based on polystyrene–PAMAM dendritic polymer electrospun nanofibers. *Talanta*, v. 260, 124630, 2023. https://doi.org/10.1016/j.talanta.2023.124630.

Robbins, A. H.; Miller, W. C. *Circuit analysis: theory and practice*. 5. ed. Delmar Cengage Learning, 2013.

Sattari, M. A.; Hayati, M. Accurate and non-contact measurement of volume percentages of oil-water fluids using microstrip sensors independent of the volume of sample using artificial neural network. *Flow Measurement and Instrumentation*, v. 97, 102621, 2024. https://doi.org/10.1016/j.flowmeasinst.2024.102621.

Tian, M. et al. Fatal methanol poisoning with different clinical and autopsy findings: case report and literature review. *Legal Medicine*, v. 54, 2022. https://doi.org/10.1016/j.legalmed.2021.101995.

Tonezzer, M. et al. Nanosensor based on thermal gradient and machine learning for the detection of methanol adulteration in alcoholic beverages and methanol poisoning. *Sensors*, v. 22, n. 15, 5554, 2022. https://doi.org/10.3390/s22155554.

Vuković Rukavina, A. Hand-held unit for liquid-type recognition, based on interdigital capacitor. *Measurement*, v. 51, p. 289–296, 2014. https://doi.org/10.1016/j.measurement.2014.02.005.

Yang, L.-J.; Yang, X.-Q.; Huang, K.-M.; Shang, H.; Jia, G.-Z. Experimental and theoretic study of the dielectric properties of ethanol + methanol mixtures. *Journal of Solution Chemistry*, v. 39, n. 4, p. 473–481, 2010. https://doi.org/10.1007/s10953-010-9513-1.

Yi, C. et al. Identification of liquor adulteration by Raman spectroscopy method based on ICNAFS. *Spectrochimica Acta Part A: Molecular and Biomolecular Spectroscopy*, v. 317, 124391, 2024. https://doi.org/10.1016/j.saa.2024.124391.

Zimmerman, N.; Presto, A. A.; Kumar, S. P. N. et al. A machine learning calibration model using random forests to improve sensor performance for lower-cost air quality monitoring. *Atmospheric Measurement Techniques*, v. 11, p. 291–313, 2018. https://doi.org/10.5194/amt-11-291-2018.